Article

Analysis of the Effect of Temperature on the Sound Transmission Loss of a Curved Plate

Guowei Zhang [1], Jianmin Ge [1],*, Shiquan Cheng [1], Tianyu Zhao [1] and Shu Liu [2]

1   Institute of Acoustics, School of Physics Science and Engineering, Tongji University, Shanghai 200092, China
2   Appraisal Center for Environment & Engineering, Ministry of Ecology and Environment, Beijing 100012, China
*   Correspondence: 1710869@tongji.edu.cn

Abstract: Curved structures are used in many engineering applications. Temperature affects the performance of structural vibration and acoustics and can damage the equipment when its effects are severe. A theoretical model of the sound transmission loss (STL) of a simply supported curved plate considering the effect of temperature was established. Moreover, a numerical solution was obtained using the modal superposition method. The finite element results were compared to validate the theoretical model. The effects of temperature and acoustic loading on the modal frequency and STL were considered, and the variation laws of the radius of curvature, opening angle, and loss factor on the STL were analyzed. The results showed that the modal frequency increased with decreasing temperature, the frequency ratio of the same-order modal frequency varied approximately linearly with temperature, and the trough of the STL shifted toward high frequencies. The pitch angle substantially influenced the STL, whereas the azimuth angle was negligible. A larger radius increased the effect of temperature. In addition, an increase in the opening angle formed an aggregation of STL at (1, 1)-order modal frequencies. The loss factor affects only the amplitude of the trough position of the STL. Therefore, the proposed theoretical model can aid in the vibroacoustic design of curved plates in a thermal environment.

Keywords: sound transmission loss; curved plate; thermal environment

1. Introduction

Curved-plate structures are increasingly used in various engineering applications, including aircraft, submarines, and construction equipment [1–3]. However, the working environments of these devices are often accompanied by high or low temperatures, which leads to changes in the functional properties of the structure [4,5]. With increasing sensitivity to the acoustic environment, increasing attention is paid to the acoustic properties of curved panels. Therefore, it is paramount to investigate the sound transmission loss (STL) of a curved plate under the influence of temperature gradients.

Many theoretical, experimental, and simulation analyses have been performed on the acoustic vibration characteristics of curved plates [6–9]. Oliazadeh and Farshidianfar [10] modeled the STL of double and triple shells based on Donnell's shell theory and compared the results with those obtained using Love's theory. The results showed that Donnell's theory produces higher accuracy in the high-frequency region. Koval and Leslie [11] analyzed the effect of a pressure difference on the STL according to the Donnell–Mushtari column and shell theory. The theoretical results showed that increasing the pressure decreases the STL of the entire frequency band while leading to a lower critical frequency. Based on the harmonic expansion method and the principle of virtual work, Wang and Ma [12] developed a theoretical model of STL for a composite structure that was coupled with a curve shell sandwich structure and acoustic metamaterials, and the effects of geometric and material parameters on the STL were discussed. Liu et al. [13] used the impedance method to investigate the effect of ribs and beams on the STL of curved plates. The authors

verified the correctness of the theory through experiments. The results showed that for plates with large curvature, the influence of the ring reinforcement method on the STL was minimal. Parrinello et al. [14] proposed a transfer matrix method for calculating the STL of multilayered cylindrical shells, which was capable of dealing with anisotropic, poroelastic, and heterogeneous cylinders and avoided the need for a homogeneous equivalent model. Daneshjiou et al. [15] developed a theoretical model for the STL of multilayer cylindrical shells made of composite materials under plane-wave incidence and analyzed the effects of the Mach number, aircraft flight altitude, and stacking order of materials on the STL. Based on the first-order shear deformation theory (FSDT), Thongchom et al. [16] developed a vibroacoustic coupling equation for a sandwiched cylindrical shell using Hamilton's principle, and the effects of the external flow and the honeycomb sandwich parameters on the STL were analyzed. Gong and Ge [17] established a theoretical model for the STL of a double-layered curved-plate cavity structure based on the fluctuation theory, analyzed the effects of different radii on the STL, and provided guidance for the optimal design of Maglev portholes using the model. Moreover, numerous researchers have studied the effects of temperature on the acoustic and vibration characteristics of structures [18–22]. Based on the fluctuation and temperature field theories, Zhang and Ge [23] investigated the modal frequencies and acoustic radiation of curved plates under simply supported boundary conditions using the modal superposition method. The authors studied the effects of temperature on various modal frequencies and radiation efficiency. Li et al. [24] established a model for the STL of a sandwich plate in a thermal environment based on Hamilton's principle; the accuracy of the model was verified by experiments, and the analysis of the results showed that the STL was more sensitive to temperature in the low-frequency range. Xin et al. [25] derived the thermoacoustic response of a rectangular simply supported flat plate in a thermal environment, verified the accuracy of the model using the finite element method, and studied the effects of the temperature difference and thermal convection on the STL and modal frequency based on the theoretical model. Haddadpour et al. [26] established the vibration control equations of a thin shell with a functional gradient under thermal load excitation based on the thin-shell theoretical model developed by Love, which was solved using the Galerkin method, and analyzed the effect of temperature on the natural frequency. The results showed that an increase in temperature decreased the natural frequency, but at a certain value of temperature, the natural frequency changed abruptly, which was mainly due to the temperature changing the wave number of the lowest natural frequency. Guo et al. [27] established a model for the STL of a double-layered rectangular sandwich panel in a thermal environment and calculated the thickness ratio of the incident- and transmitted-side rectangular panels based on the theoretical model. The results showed that the average STL under a 2 °C temperature gradient was largest when the thickness ratio of the rectangular panels on the two sides was 1.9.

The literature shows that few studies have been conducted on the performance of curved plates under temperature effects. In particular, most current research relies on the traditional elastic mechanics model to directly calculate the deflection in the dynamic equations of curved plates. The reason is that the complexity of the equation is difficult to solve. Therefore, this limitation is overcome in this study by simplifying dynamical equations by neglecting the shear force, plane displacement, and plane inertia according to the Donnell theory. In addition, the effect of temperature is considered, and the vibroacoustic performance of the curved plate is directly focused on through the solution of the modal superposition method.

In this study, based on the fluctuation and heat conduction theories, a theoretical model of the STL of a curved plate under simply supported boundary conditions when subjected to temperature and acoustic loads was established, considering the effect of temperature/thermal stress. The modal superposition method was used to solve the theoretical model, and the effects of the opening angle, radius of curvature, temperature, and acoustic incidence angle on the modal frequency and STL were analyzed.

This paper is organized as follows. The next section discusses the development of the theoretical model of the STL of curved plates in a thermal environment. In the Section 3, the theoretical results of modal frequencies and the STL are compared with the results of the finite element method to validate the model. Furthermore, based on the theoretical model, the effects of temperature on the modal frequency and STL are analyzed, as well as the effects of the pitch angle, azimuth angle, radius of curvature, opening angle, and loss factor on the STL. Finally, the conclusions are presented.

2. Theoretical Model

The model of an open-ended curved plate simply supported on all sides and subjected to acoustic excitation in the temperature field is shown in Figure 1. For the sake of computational simplicity, the model was developed using the (R, θ, L) columnar coordinate system. The curved plate's radius of curvature is R_0, its thickness is h, the circle's angle is θ_0, and its length in the axial direction is L_0. The internal part of the plate is concave, the internal temperature is T_2, the external side of the plate is convex, and the external temperature is T_1. The pitch angle of the acoustic wave is φ, and the azimuth angle is ξ.
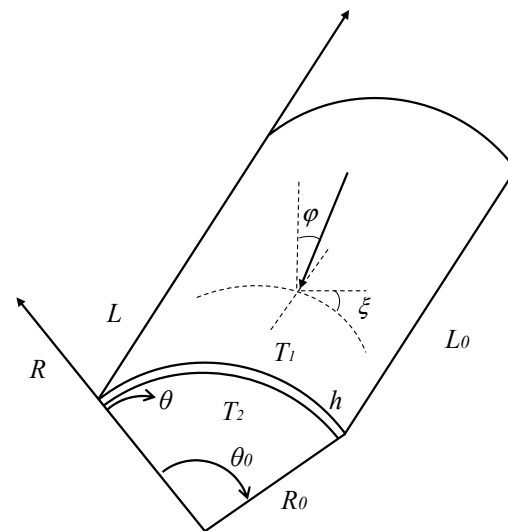
Figure 1. Schematic of the structure of the acoustic transmission arc plate in the temperature field.

The curved plate is assumed to be subjected to no thermal stress at the reference temperature (T_0). The internal temperature of the structure changes evenly throughout the thickness direction when exposed to a thermal environment.

2.1. Thermal Stress Analysis

Assuming that the curved plate is stress-free at temperature T_0, the stress state of the plate changes when the temperature changes to T due to the resulting thermal stress. In the direction along the radius, the relationship between density and temperature, according to Fourier's law of heat conduction, is as follows:

$$\rho C \frac{\partial T}{\partial t} = \kappa \frac{\partial^2 T}{\partial R^2}, \tag{1}$$

where R is the thickness direction, t is the time, ρ is the density of the medium, C is the specific heat coefficient, and κ is the heat transfer coefficient. Assuming that the inner concave side of the plate has a temperature T_2, and the outer convex side of the plate has a temperature T_1, the temperature boundary condition is as follows:

$$R = R_0 : \quad T = T_2, \tag{2}$$

$$R = R_0 + h : \quad T = T_1. \tag{3}$$

According to Equations (2) and (3), one solution of Equation (1) is

$$T(R) = \frac{T_1 - T_2}{h}(R - R_0) + \frac{T_1 + T_2}{2}. \tag{4}$$

The thermoelasticity of the plate can be described by a planar stress condition, which assumes a uniform variation in temperature with the thickness of the thin plate. The two-dimensional stress is a function of the variables L and θ. The radial stress is zero [28]. The stress–displacement relationship in the temperature field can be expressed as follows:

$$\sigma_\theta = \frac{E}{1 - v^2}[(\varepsilon_\theta + v\varepsilon_L) - \alpha(1 + v)(T - T_0)], \tag{5}$$

$$\sigma_L = \frac{E}{1 - v^2}[(\varepsilon_L + v\varepsilon_\theta) - \alpha(1 + v)(T - T_0)], \tag{6}$$

$$\tau_{\theta L} = \frac{E}{1 + v}\varepsilon_{\theta L}, \tag{7}$$

where α is the coefficient of thermal expansion of the material, E is Young's modulus, and v is Poisson's ratio.

Assuming that the thermal environment leads to a uniform increase in the in-plane temperature of the plate, the thermal load here does not cause any in-plane displacement, given the boundary conditions. Therefore, Equations (5)–(7) can be simplified as follows:

$$\sigma_\theta = -\frac{E\alpha T(z)}{1 - v}, \tag{8}$$

$$\sigma_L = -\frac{E\alpha T(z)}{1 - v}, \tag{9}$$

$$\tau_{\theta L} = 0, \tag{10}$$

By integrating Equations (8)–(10) in the thickness direction, the thermal stress can be determined as follows:

$$\begin{Bmatrix} N_\theta \\ N_L \\ N_{\theta L} \end{Bmatrix} = \int_{-\frac{h}{2}}^{+\frac{h}{2}} \begin{Bmatrix} \sigma_\theta \\ \sigma_L \\ \tau_{\theta L} \end{Bmatrix} dR = \begin{Bmatrix} -\frac{\alpha E(T_1 + T_2)h}{2(1-v)} \\ -\frac{\alpha E(T_1 + T_2)h}{2(1-v)} \\ 0 \end{Bmatrix}, \tag{11}$$

where N_θ, N_L, and $N_{\theta L}$ are the thermal stresses in the three directions.

2.2. Vibration Theory of a Simply Supported Curved-Plate Structure in a Thermal Environment

Flügge's [29] theory provides vibration equations based on the thin-shell assumption. However, because the theory considers the related shear and inertial forces as well as the loads in all directions, the equations are complicated and inconvenient to calculate. In this study, based on the simplified theory of Donnell [30], the dynamic equation neglects the shear forces, plane displacement, and plane inertia. In addition, the effects of sound pressure fluctuations and thermal stress are considered; therefore, the vibration control equation of the curved plate is as follows:

$$D\nabla^4 w + \nabla_1^2 f + \rho h \frac{\partial^2 w}{\partial t^2} = j\omega(\rho_1 \Phi_1 - \rho_2 \Phi_2) + N_\theta \frac{\partial^2 w}{R^2 \partial \theta^2} + N_L \frac{\partial^2 w}{\partial L^2} + 2N_{\theta L} \frac{\partial^4 w}{R^2 \partial \theta^2 \partial L^2}, \tag{12}$$

where j is the imaginary part, w is the deflection, ρ_1 and ρ_2 are the air densities on the incident and radiating sides of the curved plate, respectively, ρ is the plate density, and Φ_1

and Φ_2 are the acoustic velocity potential functions on the incident side and the radiating side of the curved plate, respectively. f is the Airy stress function replacing the film stress and satisfying the coordination equation [30].

$$Eh\nabla_1^2 w - \nabla^4 f = 0. \tag{13}$$

The plate's bending stiffness (D) is as follows:

$$D = \frac{Eh^3(1 + j\eta)}{12(1 - v^2)}, \tag{14}$$

where η is the loss factor of the plate. ∇ is the Laplace operator, denoted as follows:

$$\nabla^2 = \frac{\partial^2}{\partial L^2} + \frac{1}{R^2}\frac{\partial^2}{\partial \theta^2}. \tag{15}$$

∇_1 is the variational Laplace operator, denoted as follows:

$$\nabla_1^2 = \frac{1}{R}\frac{\partial^2}{\partial L^2}. \tag{16}$$

Joining Equations (12)–(16) results in the vibration control equation of the curved plate in a thermal environment.

$$D\nabla^8 w + Eh\nabla_1^4 w + \rho h \nabla^4 \frac{\partial^2 w}{\partial t^2} = \\ \nabla^4 \left(j\omega(\rho_1\Phi_1 - \rho_2\Phi_2) + N_\theta \frac{\partial^2 w}{R^2 \partial \theta^2} + N_L \frac{\partial^2 w}{\partial L^2} + 2N_{\theta L}\frac{\partial^4 w}{R^2 \partial \theta^2 \partial L^2} \right). \tag{17}$$

2.3. Sound Transmission Loss

According to the fluctuation theory, the velocity potential functions of the incident and radiated sound fields can be expressed as follows:

$$\Phi_1(\theta, L, R; t) = Ie^{-j(k_\theta\theta + k_L L + k_R(R-R_0) - \omega t)} + \beta e^{-j(k_\theta\theta + k_L L - k_R(R-R_0) - \omega t)}, \tag{18}$$

$$\Phi_2(\theta, L, R; t) = \varepsilon e^{-j(k_\theta\theta + k_L L + k_R(R-R_0) - \omega t)}. \tag{19}$$

The wave numbers in each direction are $k_\theta = k_0 sin\varphi cos\xi$, $k_L = k_0 sin\varphi sin\xi$, and $k_R = k_0 cos\varphi$, where $k_0 = \omega/c$. Because the boundary conditions are simply supported, at the plate's outer edge, both the bending moment and displacement are zero. Therefore, the mathematical description of the curved plate is as follows:

$$\theta = 0, \theta_0 : w = 0, \ \frac{\partial^2 w}{\partial \theta^2} = 0, \tag{20}$$

$$L = 0, L_0 : w = 0, \ \frac{\partial^2 w}{\partial L^2} = 0. \tag{21}$$

According to Equations (20) and (21), the deflection (w) can be expressed as a double trigonometric expression, as follows:

$$w(\theta, L, t) = \sum_{m=1}^{\infty}\sum_{n=1}^{\infty} A_{mn}\varphi_{mn}e^{j\omega t}, \tag{22}$$

where m and n represent the number of waves in the circumferential and axial directions, respectively, and A_{mn} is the modal array coefficient. φ_{mn} is the modal function, whose expression is as follows:

$$\varphi_{mn} = \sin\frac{m\pi\theta}{\theta_0}\sin\frac{n\pi L}{L_0}. \tag{23}$$

According to the deflection equation, Equation (22), the velocity potential function of the sound pressure can be expressed as follows:

$$\Phi_1(\theta, L, R; t) = \sum_{m,n} I_{mn}\varphi_{mn}e^{-j(k_R(R-R_0)-\omega t)} + \sum_{m,n} \beta_{mn}\varphi_{mn}e^{-j(-k_R(R-R_0)-\omega t)}, \quad (24)$$

$$\Phi_2(\theta, L, R; t) = \sum_{m,n} \varepsilon_{mn}\varphi_{mn}e^{-j(k_R(R-R_0)-\omega t)}, \quad (25)$$

where I_{mn} and β_{mn} are the incident and reflected wave amplitudes, respectively, and ε_{mn} is the radiation wave amplitude. I_{mn}, β_{mn}, and ε_{mn} are related to the original coefficients as follows:

$$\lambda_{mn} = \frac{4}{\theta L} \int_0^\theta \int_0^L \lambda e^{-j(k_\theta\theta + k_L L)} \sin\frac{m\pi\theta}{\theta_0} \sin\frac{n\pi L}{L_0} d\theta dL, \quad (26)$$

where λ refers to the coefficients I, β, and ε in general. At the air-and-plate intersection, the following equation is obtained according to the condition of velocity continuity.

$$R = R_0 + h: \qquad -\frac{\partial\Phi_1}{\partial R} = j\omega w \ , \quad (27)$$

$$R = R_0: \qquad -\frac{\partial\Phi_2}{\partial R} = j\omega w \ . \quad (28)$$

Substituting Equations (24) and (25) into Equations (27) and (28), respectively, we obtain the following:

$$\beta_{mn} = I_{mn}e^{-2jk_{1R}h} - \frac{\omega}{k_{1R}}A_{mn}e^{-jk_{1R}h}, \quad (29)$$

$$\varepsilon_{mn} = \frac{\omega A_{mn}}{k_{2R}}. \quad (30)$$

The conjunction of Equations (17) and (30) gives

$$A_{mn}D\nabla^8\varphi(\theta, L) + A_{mn}Eh\nabla_1^4\varphi(\theta, L) - \omega^2\rho h A_{mn}\nabla^4\varphi(\theta, L) = \\ j\omega\nabla^4\varphi(\theta, L)\left[\rho_1 I_{mn}e^{-jk_{1R}h} + \rho_1\beta_{mn}e^{jk_{1R}h} - \rho_2\varepsilon_{mn}\right] \quad (31)$$

Substituting Equations (22) and (23) into Equation (12), with $\Phi_1 = \Phi_2 = 0$, the natural frequency can be calculated as follows:

$$\omega_{mn} = \sqrt{\frac{D}{\rho h}\left[\left(\frac{n\pi}{L_0}\right)^2 + \frac{1}{R^2}\left(\frac{m\pi}{\theta_0}\right)^2\right]^2 + \frac{\frac{Eh}{R^2}\left(\frac{n\pi}{L_0}\right)^4}{\rho h\left[\left(\frac{n\pi}{L_0}\right)^2 + \frac{1}{R^2}\left(\frac{m\pi}{\theta_0}\right)^2\right]^2} + \frac{N_\theta}{\rho h R^2}\left(\frac{m\pi}{\theta_0}\right)^2 + \frac{N_L}{\rho h}\left(\frac{n\pi}{L_0}\right)^2}. \quad (32)$$

According to Equations (31) and (32), the modal coefficient (A_{mn}) can be calculated as follows:

$$A_{mn} = \frac{2j\omega\rho_1 I_{mn}e^{-jk_{1R}h}}{(\omega_{mn}^2 - \omega^2)\rho h + j\omega^2(\rho_1/k_{1R} + \rho_2/k_{2R})}. \quad (33)$$

The sound power transmission coefficient is the ratio of the radiated sound power to the incident sound power and is expressed as follows:

$$\tau(\varphi, \xi) = \frac{\sum\limits_{m=1}^\infty \sum\limits_{n=1}^\infty \rho_2|\varepsilon_{mn}|}{\sum\limits_{m=1}^\infty \sum\limits_{n=1}^\infty \rho_1|I_{mn} + \beta_{mn}|}. \quad (34)$$

For random incidence, the azimuth and pitch intervals are integrated separately, and the sound power transmission coefficient is [31]

$$\tau_{di} = \frac{\int_0^{\pi/4} \int_0^{\varphi_{\max}} \tau(\varphi,\xi) \sin\varphi \cos\varphi \sin\xi \cos\xi \, d\varphi \, d\xi}{\int_0^{\pi/4} \int_0^{\varphi_{\max}} \sin\varphi \cos\varphi \sin\xi \cos\xi \, d\varphi \, d\xi}. \tag{35}$$

The literature [32] reports that the theoretical value agrees better with the measurement results when the upper limit of integration is 78° or 85°. In this study, φ_{max} takes the value of 78°.

3. Model Validation

The finite element method was used to calculate the modal frequencies and STL of the curved plate and verify the accuracy of the model. Two different temperature conditions were used, assuming that the temperatures on the incident and radiating sides of the curved plate are $T_1 = 0$ °C, $T_2 = 0$ °C and $T_1 = -10$ °C, $T_2 = 0$ °C, respectively. The material parameters, dimensions, and thermodynamic parameters of the curved plate and the parameters of the air medium are listed in Table 1 [33]. Because the temperature range considered in this study was not large, the negligible variation in the material parameters was not considered. The modal frequency was solved using ANSYS, and the mode with thermal stress was used for the calculation. A simply supported boundary was set as the boundary condition. The modal calculation result file "rst" of ANSYS was imported into the acoustic calculation software ACTRAN to calculate the STL. The simulation model in ACTRAN is shown in Figure 2. On the radiation side, a three-dimensional acoustic cavity mesh was created to simulate the air domain of acoustic wave propagation. Moreover, the outside of the cavity was given infinite element boundary properties to absorb acoustic waves and calculate the radiated sound power. According to the 1/6 [34] wavelength principle, the maximum length of the acoustic cavity unit was 20 mm, which corresponded to the calculation range of 2000 Hz. The calculation frequency range for the STL was set to 20–1000 Hz, the calculation step was 5 Hz, and it took 10 h 17 min for the computer to perform one calculation.

Table 1. Structural dimensions and material parameters of the curved plate.

Parameters	Symbols and Values
Opening angle	$\theta_0 = 60°$
Radius of curvature	$R_0 = 1$ m
Axial length	$L_0 = 1.5$ m
Thickness	$h = 0.01$ m
Young's modulus	$E = 71$ GPa
Poisson's ratio	$v = 0.33$
Density	$\rho = 2700$ kg/m^3
Specific heat	$C = 880$ J/(kg·K)
Thermal expansion coefficient	$\kappa = 236$ W/(m·K)
Coefficient of thermal conductivity	$\alpha = 2.3 \times 10^{-5}$ m/(m·K)
Air density	$\rho = 1.225$ kg/m^3
Speed of sound	$c_0 = 340$ m/s
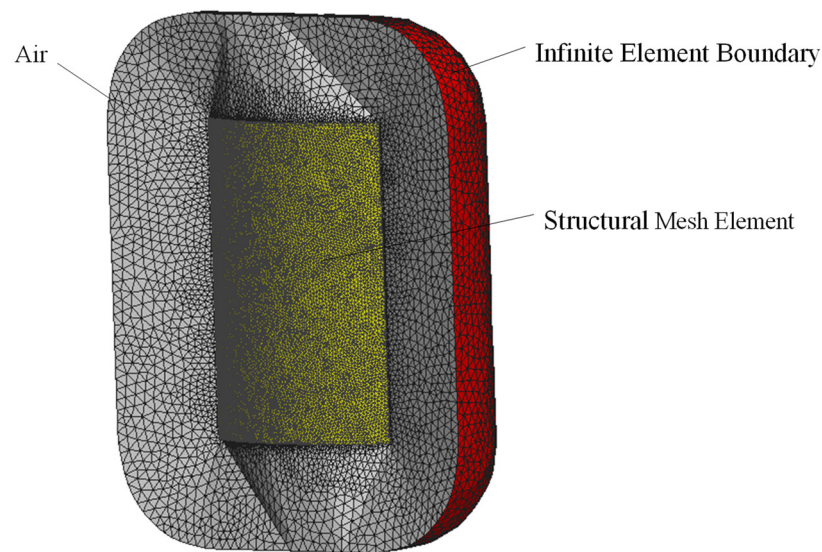
Figure 2. Simulation model for STL.

The theoretical calculations were performed using the modal superposition method, which satisfied a sufficient number of terms and ensured the convergence of the numerical predictions. The existing results show that if a term is found and the level solution converges within the target frequency, then the level solution of this term converges below the target frequency [35]. In this calculation, f = 10,000 Hz was chosen to check for convergence. For the following analysis, the angle of incidence was set to $0°$. In the traversal calculation term, the values of m and n were always kept equal. The results are shown in Figure 3. When the number of terms is 20, the result of the series stabilizes, and the sum result of the series can converge as the number of terms continues to increase. This shows that the convergence of the theoretical results can be guaranteed when both m and n take values greater than 20. To simplify the calculation and ensure convergence, in this study, we set $m = n = 50$, and the partial terms in Equation (24) were summed separately for 2500 terms. The calculation quantities and computation times were coherent.
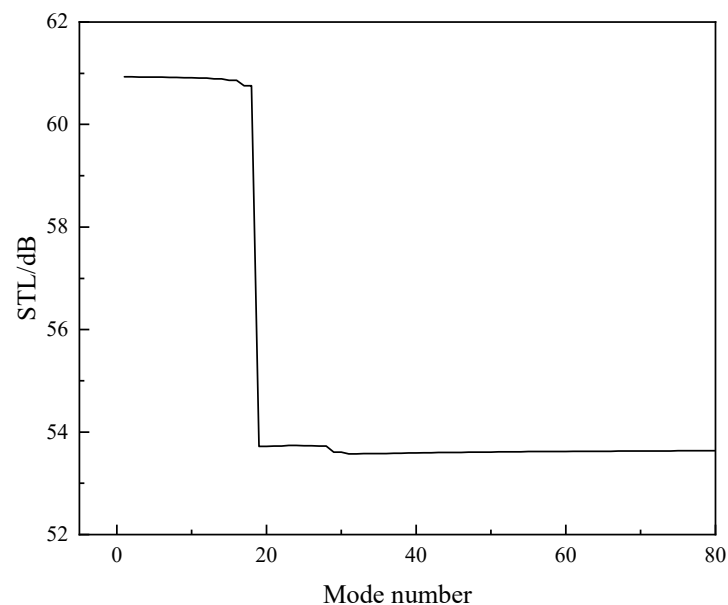

Figure 3. Level convergence verification.

The results of the theoretical calculation and simulation of the modal frequency of the curved plate are shown in Figure 4. The theoretical and simulation results of the STL are

shown in Figure 5. In particular, the acoustic wave incidence was random. Note that the theoretical calculation results of both the modal frequency and STL agree well with the simulation results under different temperature conditions, indicating that the theoretical model can be used to analyze the modal frequency and STL of a curved plate.
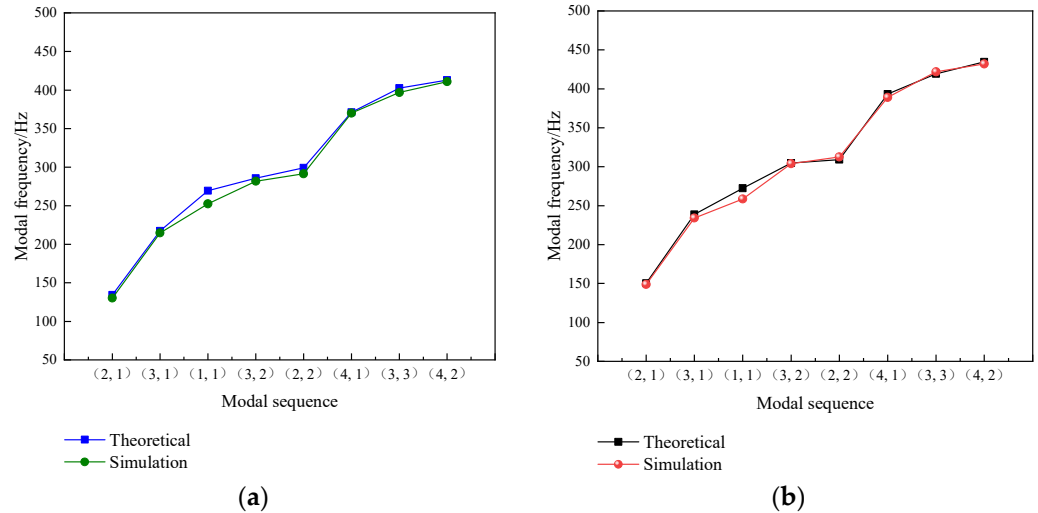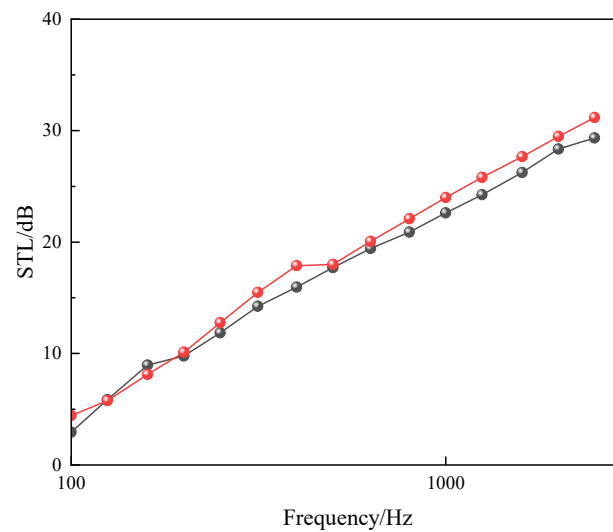

Figure 4. Comparison of the theoretically calculated and simulated values of the modal frequencies. (**a**) $T_1 = 0\ °C$, $T_2 = 0\ °C$. (**b**) $T_1 = -10\ °C$, $T_2 = 0\ °C$.
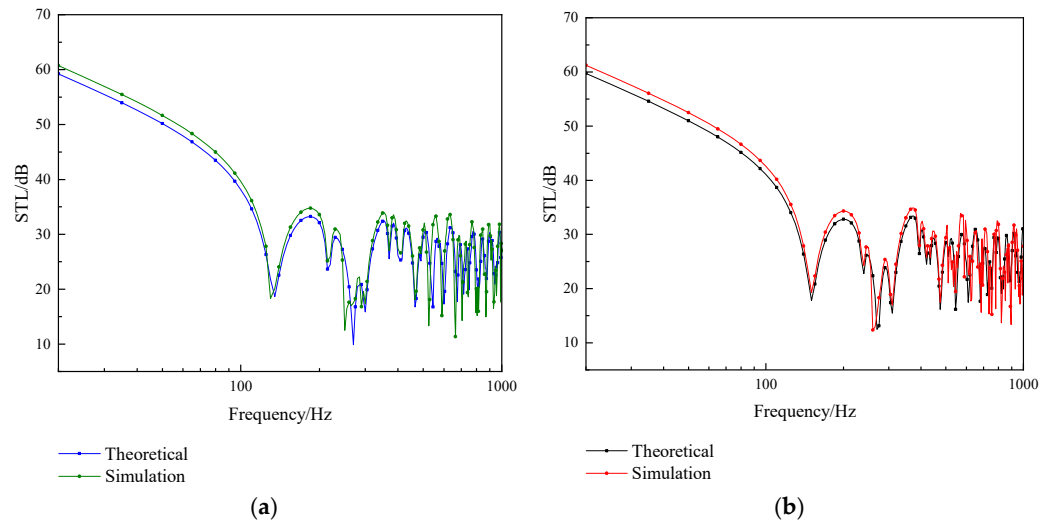
Figure 5. Comparison of the theoretically calculated and simulated values of STL. (**a**) $T_1 = 0\ °C$, $T_2 = 0\ °C$. (**b**) $T_1 = -10\ °C$, $T_2 = 0\ °C$.

Furthermore, to compare the differences between the present study and previous solutions, the parameters in [13] were used. Thus, the results of the theoretical calculations in this study and those in [13] are given in Figure 6. The figure shows that the present study agrees well with the calculation results in [13].

Figure 6. Comparison of the theoretically calculated STL with that using parameters from a previous study, black dotted line: Ref. [13], red dotted line: present.

4. Numerical Results and Analysis

Based on the theoretical model in the previous section, the variation in the modal frequencies and STL of the curved plate at different temperature gradients was analyzed. In addition, the effects of the acoustic incidence angle, radius of curvature, opening angle, and loss factor on the STL were considered.

4.1. Effect of Temperature

When an aircraft flies at a high altitude, the ambient temperature is often low. To further analyze the effect of low temperature on modal frequencies, assuming that the internal temperature ($T_2 = 0$ °C) of the curved plate is kept constant, the modal frequency distribution was considered when the external temperature was $T_1 = -10, -20, -30, -40$, and -50 °C. Table 2 lists the modal frequencies for six different temperature gradients, and the variation in each order of mode with different temperatures is shown in Figure 7. Taking $T_1 = 0$ °C as the base condition, Table 2 shows that at $T_1 = -20$ and -30 °C, the (2, 2)-order mode and (3, 2)-order mode change the order of occurrence as the modal frequencies go from small to large compared with $T_1 = 0$ °C; at $T_1 = -40$ and -50 °C, the (3, 2)-order mode and (1, 1)-order mode change the order of occurrence as the modal frequencies go from small to large; and the (3, 3)-order mode and (4, 2)-order mode also change the order of occurrence. Note that a decrease in temperature leads to a change in the order of mode shapes, and the more the temperature decreases, the more the mode shapes are changed. Simultaneously, the same-order modal frequency gradually increases with a decrease in temperature.

Table 2. Modal frequencies at different temperature gradients (Hz).

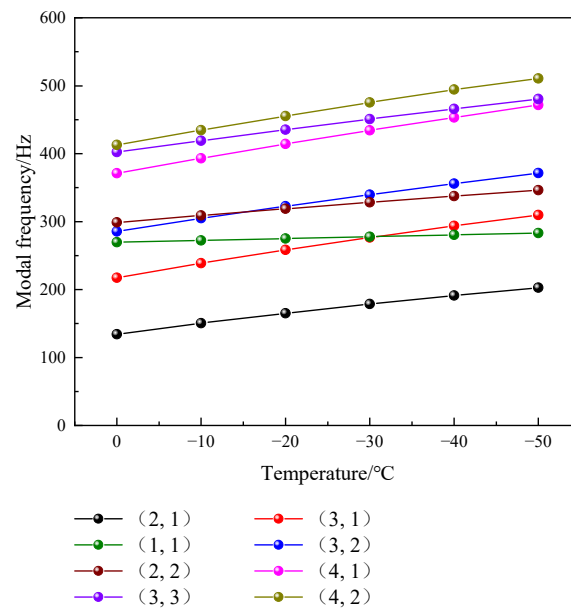| Sequence	$T_1 = 0$ °C	$T_1 = -10$ °C	$T_1 = -20$ °C	$T_1 = -30$ °C	$T_1 = -40$ °C	$T_1 = -50$ °C
(2, 1)	134.2	150.5	165.1	178.5	191.0	202.7
(3, 1)	217.2	238.6	258.3	276.5	293.6	309.8
(1, 1)	269.5	272.3	275.1	277.9	280.6	283.4
(3, 2)	285.7	304.8	322.7	339.7	355.9	371.4
(2, 2)	299.0	309.0	318.8	328.2	337.4	346.4
(4, 1)	371.1	393.3	414.3	434.3	453.4	471.8
(3, 3)	402.4	419.2	435.3	450.8	465.9	480.4
(4, 2)	412.8	434.6	455.4	475.2	494.3	510.7

Figure 7. Variation in modal frequencies of each order at different temperatures.

The frequency ratio is defined as $\gamma = f_T/f_0$, where f_T is the modal frequency under various temperature gradients, and f_0 is the modal frequency of each order at the temperature of $T_1 = 0\ {}^\circ\text{C}$. The variation in the frequency ratio of each order of modal frequency with temperature is shown in Figure 8. The figure demonstrates that each order of modal frequency varies approximately linearly with decreasing temperature. The frequency ratio of the (2, 1)-order modal frequency changes the most, with the modal frequency increasing on average by 13.7 Hz per 10 ${}^\circ\text{C}$ temperature decrease. The frequency ratio of the (1, 1)-order modal frequency decreases the least, with the modal frequency increasing on average by 2.8 Hz per 10 ${}^\circ\text{C}$ temperature decrease.
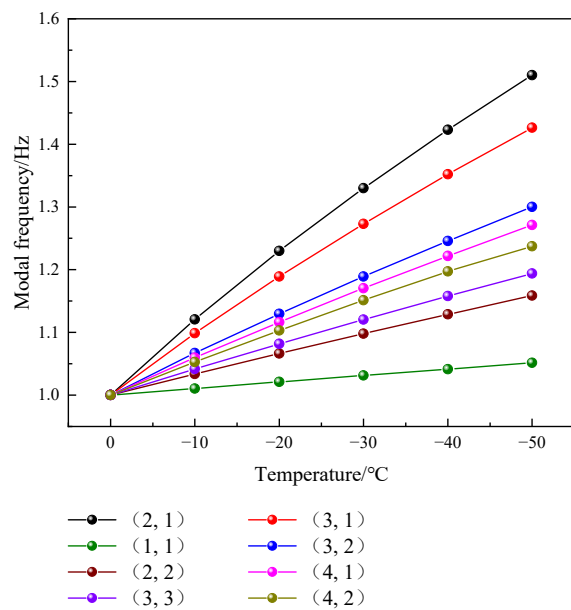

Figure 8. Variation in modal frequency with temperature for each order.

The curves of the STL with the frequency of the curved plate at different temperature gradients when the acoustic wave is vertically incident are shown in Figure 9. The figure shows that the trough position of the STL gradually shifts toward high frequencies as the temperature decreases. Moreover, these trough positions and the modal frequencies are con-

sistent. In particular, the frequencies corresponding to each trough are modal frequencies. The first four trough frequencies of the STL at T_1 = 0, −10, −20, and −30 °C correspond to the (3, 1)-, (1, 1)-, (3, 3)-, and (5, 1)-order modal frequencies at that temperature, and the first four trough frequencies of the STL at T_1 = −40 and −50 °C correspond to the (1, 1)-, (3, 1)-, (3, 3)-, and (5, 1)-order modal frequencies at that temperature. The corresponding modal frequencies at different temperatures are (odd, odd)-order modal frequencies. This is because the (odd, odd)-order modes radiate more efficiently with increasing frequency and are more easily excited [36]. As shown in Table 2, when T_1 is −40 and −50 °C, the change in temperature causes an array exchange between the (3, 1)-order mode and the (1, 1)-order mode. Therefore, the first trough position is the frequency position corresponding to the (1, 1)-order mode, and the temperature changes can cause significant changes in the STL performance of the curved plate. In low-temperature environments, the low-frequency locations, where the STL is weak at the vertical incidence of acoustic waves, shift to higher frequencies.
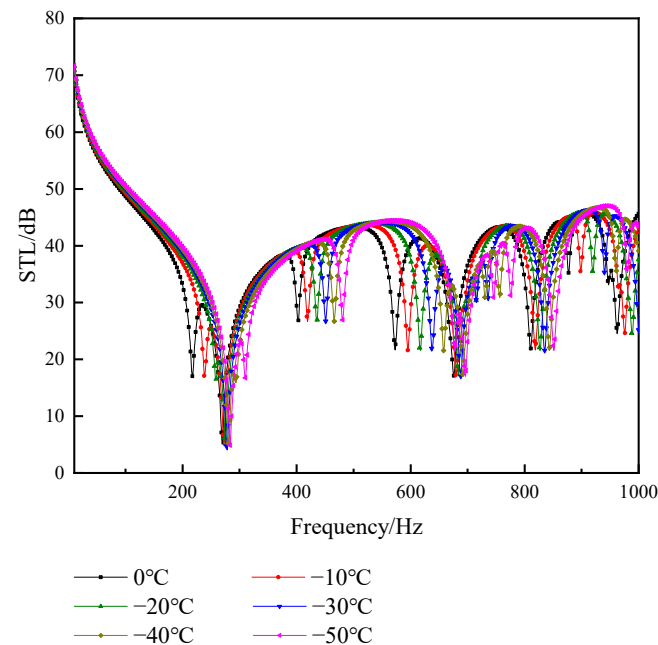
**Figure 9.** Variation in STL at different temperatures.

4.2. Effect of Pitch and Azimuth Angles

Random incidence is a desirable condition, and realistic scenarios often occur where sound waves are excited at a fixed angle. At T_2 = 0 °C and T_1 = −50 °C, the variation in STL with frequency is shown in Figure 9, where the azimuth angle is kept at 0°, and the pitch angle is set at 0°, 30°, 60°, and 90°. Figure 10 also shows that different angles of incidence of the sound waves have different effects on the STL. When the sound waves are incident at a pitch angle of 0°, the STL is the greatest in the low-frequency range, and as the angle increases, the STL in the low-frequency range decreases. The position of the trough of the STL also changes with a change in the angle of incidence. The reason is that the smaller the pitch angle, the greater the air–solid coupling mode density of the curved-plate structure. Thus, the STL deteriorates when the pitch angle increases.
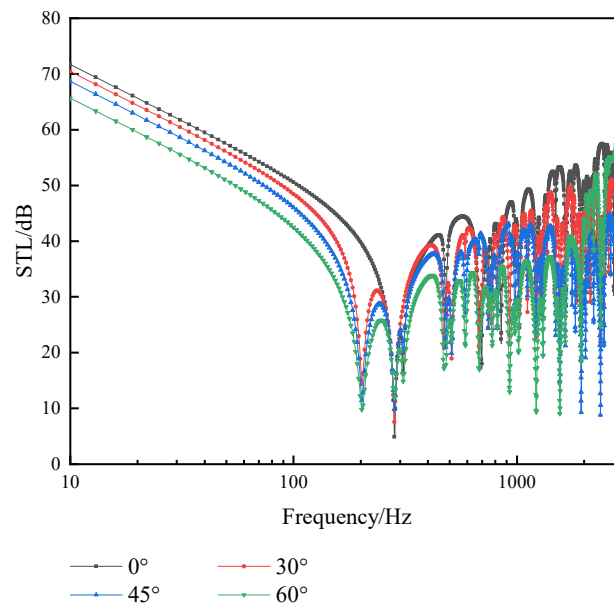
Figure 10. Effect of different pitch angles on STL.

Figure 11 shows the variation in STL with frequency for four cases, where the pitch angle is kept at 0° and the azimuth angle is 0°, 30°, 60°, and 90°. The figure shows that the STL is not affected by a change in the azimuth angle.
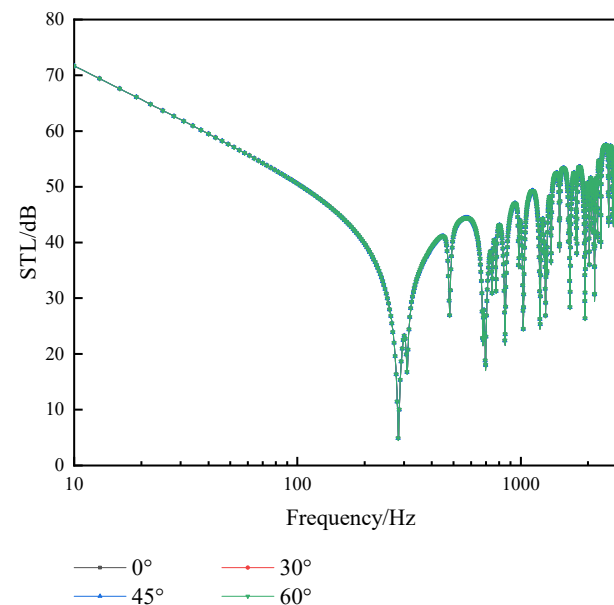

Figure 11. Effect of different azimuth angles on STL.

### 4.3. Effect of the Radius of Curvature and Opening Angle

The radius of curvature and opening angle, which are important parameters for the design of structures, are geometrical characteristics unique to curved plates rather than flat plates. The variation in STL with temperature for an opening angle of $\pi/3$ and radii of curvature of 2, 4, 8, and 10,000 m for a curved plate at the vertical incidence of acoustic waves is shown in Figure 12. The figure shows that the first trough of the STL becomes progressively smaller as the radius increases. Simultaneously, the effect of temperature on the STL is more evident in the low-frequency range. As the temperature decreases, the trough gradually shifts to a high frequency; when the curved plate approaches a flat plate, the effect of temperature on the STL is evident. This is due to the effect of the radius of

curvature, which produces membrane stress, and the effect of temperature, which produces temperature stress. As the radius increases, the membrane stress gradually decreases, and the lower the temperature, the greater the temperature stress. Thus, if the radius is large and the temperature is low, the effect of temperature is noticeable.
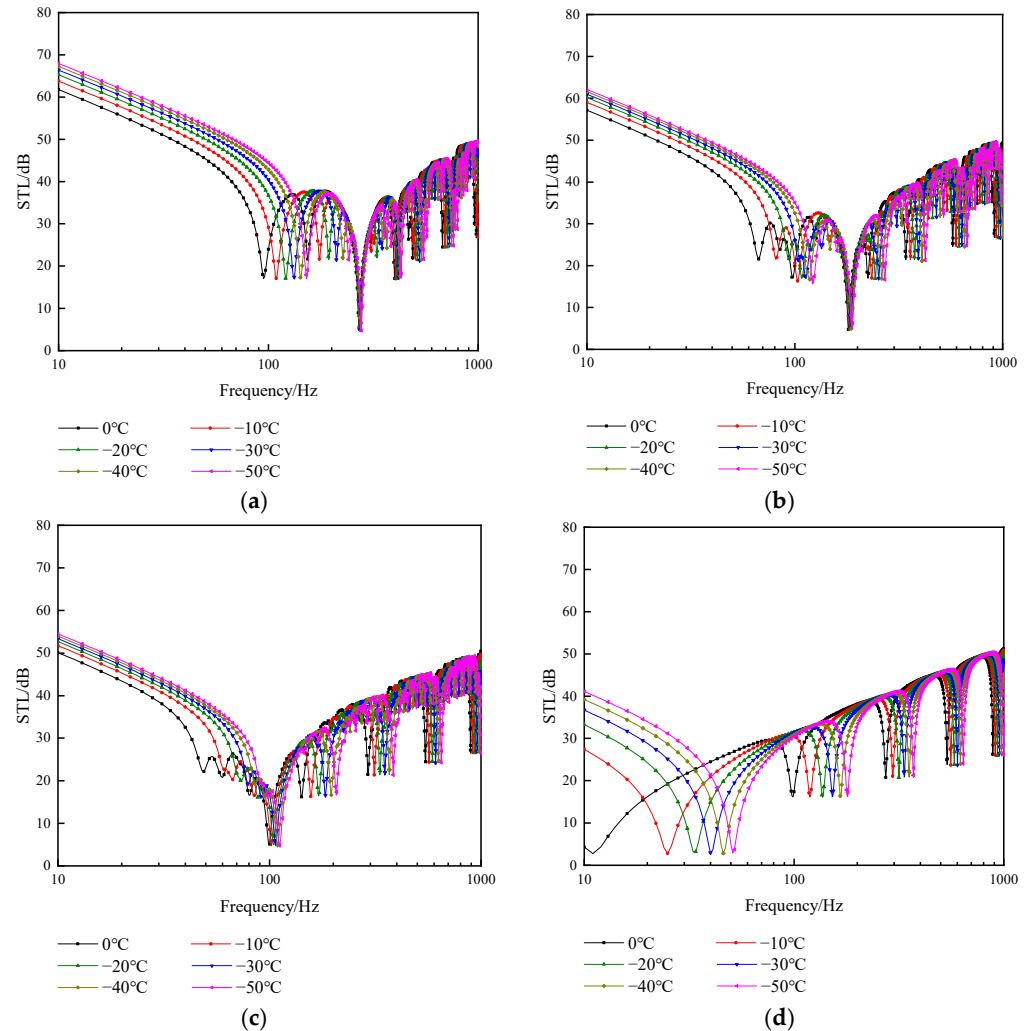
Figure 12. Influence of the temperature on STL at different radii. (**a**) $R = 2$ m. (**b**) $R = 4$ m. (**c**) $R = 8$ m. (**d**) $R = 10,000$ m.

Figure 13 shows the variation in STL of the curved plate at a radius of curvature of 1 m and opening angles of $\pi/6$, $\pi/3$, $\pi/2$, and $2\pi/3$. The figure shows that as the opening angle increases, the STL at (1, 1) modal frequencies are all in the trough position. The larger the opening angle, the more evident the aggregation effect at this position and the smaller the effect due to temperature. This is because the larger the opening angle, the farther the curved plate is from a flat state and the more pronounced the effect of curvature, intensifying the centripetal effect toward the center of the surface. As the opening angle increases, the first trough position of the STL becomes inconsistent. This is due to the change in angle, causing the distribution of modal formations to appear out of sequence. When the sound waves are incident vertically, the parity distribution of the mode shape determines the trough position of the STL.
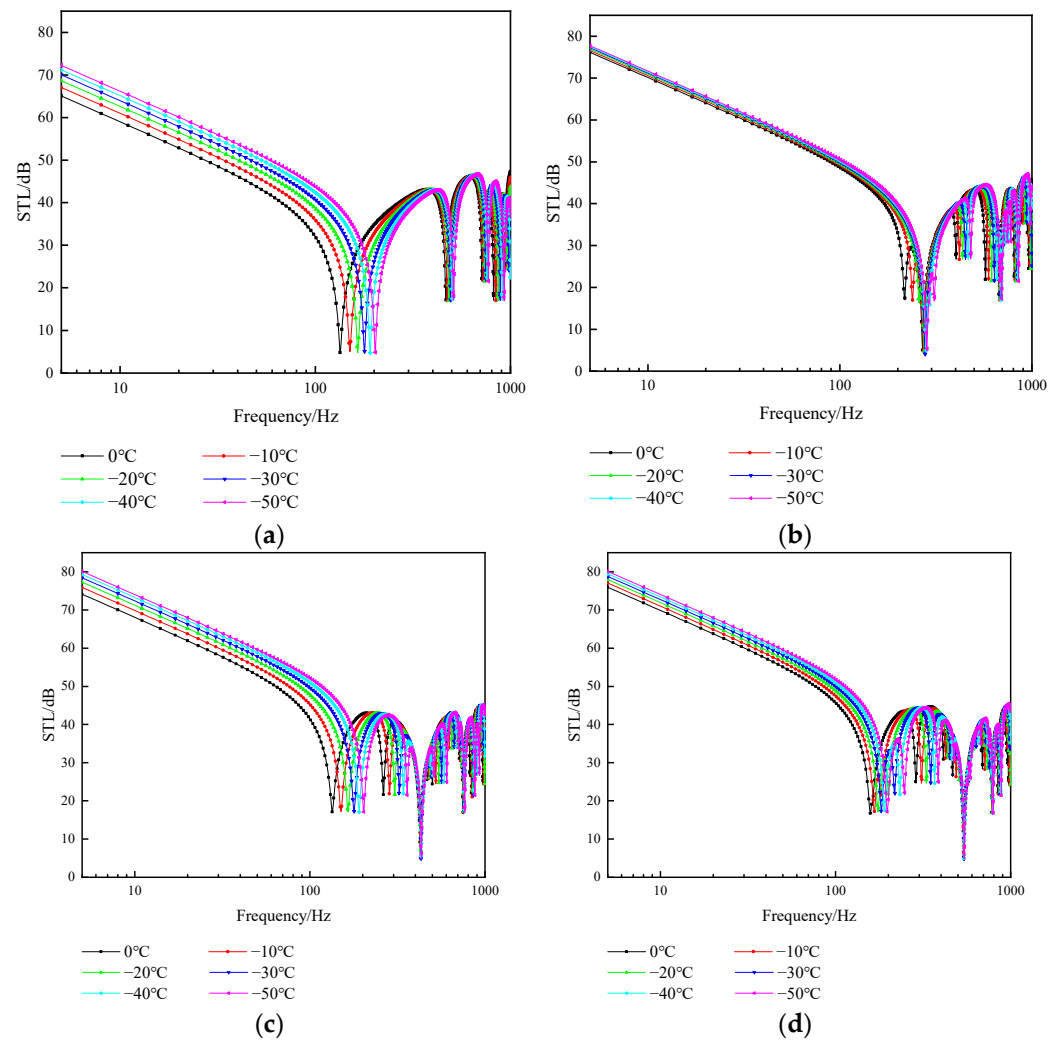
Figure 13. Influence of the temperature on STL at different opening angles. (**a**) $\theta = \pi/6$. (**b**) $\theta = \pi/3$. (**c**) $\theta = \pi/2$. (**d**) $\theta = 2\pi/3$.

4.4. Effect of Loss Factor

The loss factor of metallic materials is generally low at room temperature and varies with temperature and frequency [37,38]. To simplify the calculation, we consider the loss factor for the entire frequency band with a fixed value. Figure 14 presents the results for $T_2 = 0\ ^\circ\text{C}$ and $T_1 = -50\ ^\circ\text{C}$. When the sound waves are incident vertically, various loss factors affect the STL. As shown in Figure 14, the influence of the loss factor is also reflected in the trough position of the STL. Moreover, with an increase in the loss factor, the amplitude at the trough position increases gradually; in the non-valley position, the influence of the loss factor is less prominent.
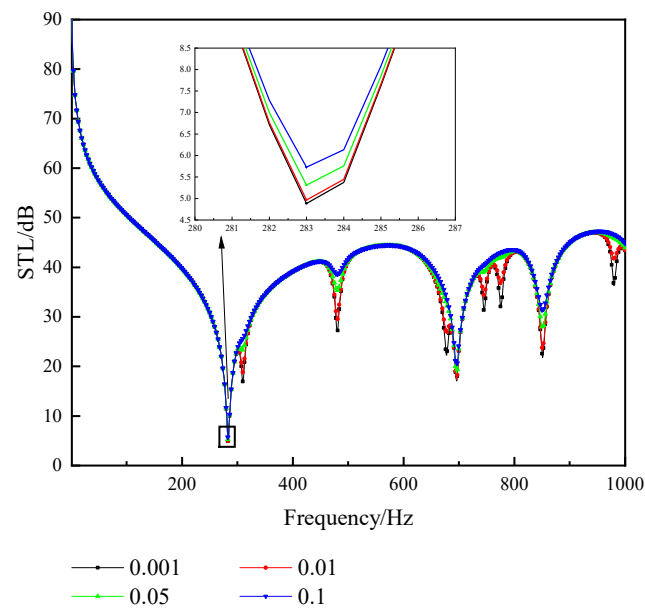
Figure 14. Effect of the different loss factors on STL.

5. Conclusions

In this study, based on the fluctuation and heat conduction theories, in conjunction with the Donnell equation for curved plates, a model of the STL of a curved plate was established under simply supported boundary conditions. The solution was obtained using the modal superposition method, and the accuracy of the model was verified using the finite element method. The following conclusions can be drawn based on the analysis of the theoretical model.

1. Temperature affects modal frequencies of different orders to different extents. For the curved plate, the minimum modal frequency is most affected by temperature, and the (1, 1)-order modal frequency is least affected by temperature. The modal frequency ratio varies approximately linearly with decreasing temperature.
2. Temperature changes cause a change in the order of appearance of the mode shapes, and the greater the temperature change, the more the order of the mode shapes changes. The effect of temperature on STL is due to temperature changing the modal frequencies.
3. The larger the radius, the more pronounced the effect of temperature on the STL. As the opening angle increases, the STL will experience an aggregation phenomenon at (1, 1)-order modal frequencies.

Author Contributions: Conceptualization, G.Z.; methodology, G.Z.; software, S.C.; validation, T.Z.; formal analysis, G.Z.; investigation, S.C.; resources, J.G.; data curation, G.Z.; writing—original draft preparation, G.Z.; writing—review and editing, G.Z.; visualization, T.Z.; supervision, J.G.; project administration, J.G.; funding acquisition, S.L. All authors have read and agreed to the published version of the manuscript.

Institutional Review Board Statement: Not applicable.

Informed Consent Statement: Not applicable.

Data Availability Statement: The data presented in this study are available on request from the corresponding author.

Conflicts of Interest: The authors declare no conflict of interest.

References

1. Zhang, Y.B.; Ren, C.Y.; Zhu, X. Research on Vibration and Sound Radiation from Submarine Functionally Graded Material Nonpressure Cylindrical Shell. *Adv. Mater. Res.* **2013**, *690–693*, 3046–3049. [CrossRef]
2. Behrens, B.; Müller, M. Technologies for Thermal Protection Systems Applied on Re-usable Launcher. *Acta Astronaut.* **2004**, *55*, 529–536. [CrossRef]
3. Sreelatha, P.R.; Mathai, A. Linear and Nonlinear Buckling Analysis of Stiffened Cylindrical Submarine Hull. *Int. J. Eng. Sci.* **2012**, *4*, 3003–3009.
4. Timoshenko, S.P.; Gere, J.M.; Prager, W. *Theory of Elastic Stability*, 2nd ed.; Dover publications, Inc.: Mineola, NY, USA, 1962; Volume 29, p. 220.
5. Qian, H.; Zhou, D.; Yin, J.; Qiu, Y. A Theoretical Investigation on the Thermal Response of Laminated Cylindrical Panel. *Arch. Appl. Mech.* **2020**, *90*, 475–493. [CrossRef]
6. Zhao, T.; Yang, Z.; Tian, W.; Chen, Z. Vibration and Acoustic Radiation Characteristics Analysis of Composite Laminated Plate in Hygrothermal Environments. *Acta Aeronaut. Astronaut. Sin.* **2017**, *38*, 221038.
7. Lee, J.H.; Kim, J. Study on Sound Transmission Characteristics of a Cylindrical Shell Using Analytical and Experimental Models. *Appl. Acoust.* **2003**, *64*, 611–632. [CrossRef]
8. Ali, N.; Sohrab, A. Optimization of Sound Transmission Loss Through a Thin Functionally Graded Material Cylindrical Shell. *Shock Vib.* **2014**, *2014*, 10. [CrossRef]
9. Gupta, P.; Parey, A. Prediction of sound transmission loss of cylindrical acoustic enclosure using statistical energy analysis and its experimental validation. *J. Acoust. Soc. Am.* **2022**, *151*, 544. [CrossRef]
10. Oliazadeh, P.; Farshidianfar, A. Analysis of Different Techniques to Improve Sound Transmission Loss in Cylindrical Shells. *J. Sound Vib.* **2017**, *389*, 276–291. [CrossRef]
11. Koval, L.R. Effect of Air Flow, Panel Curvature, and Internal Pressurization on Field-Incidence Transmission Loss. *J. Acoust. Soc. Am.* **1967**, *59*, 1379–1385. [CrossRef]
12. Wang, Y.-Z.; Ma, L. Sound insulation performance of curved sandwich structure combined with acoustic metamaterials. *J. Vib. Control* **2023**, 10775463231187694. [CrossRef]
13. Liu, B.; Feng, L.; Nilsson, A. Sound Transmission Through Curved Aircraft Panels with Stringer and Ring Frame Attachments. *J. Sound Vib.* **2007**, *300*, 949–973. [CrossRef]
14. Parrinello, A.; Kesour, K.; Ghiringhelli, G.L.; Atalla, N. Diffuse field transmission through multilayered cylinders using a Transfer Matrix Method. *Mech. Syst. Signal Process.* **2020**, *136*, 106514. [CrossRef]
15. Daneshjou, K.; Nouri, A.; Talebitooti, R. Sound Transmission Through Laminated Composite Cylindrical Shells Using Analytical Model. *Arch. Appl. Mech.* **2007**, *77*, 363–379. [CrossRef]
16. Thongchom, C.; Jearsiripongkul, T.; Refahati, N.; Roudgar Saffari, P.; Roodgar Saffari, P.; Sirimontree, S.; Keawsawasvong, S. Sound Transmission Loss of a Honeycomb Sandwich Cylindrical Shell with Functionally Graded Porous Layers. *Buildings* **2022**, *12*, 151. [CrossRef]
17. Gong, Y.; Ge, J. Investigation of Sound Insulation Performance of High-Speed Maglev Train Porthole Based on the Wave Theory. *J. Huazhong Univ. Sci. Tech.* **2020**, *6*, 57–63.
18. Chronopoulos, D.; Ichchou, M.; Troclet, B.; Bareille, O. Thermal Effects on the Sound Transmission Through Aerospace Composite Structures. *Aerosp. Sci. Technol.* **2013**, *30*, 192–199. [CrossRef]
19. Qian, G.; Li, Y. Analysis of Dynamic and Acoustic Radiation Characters for a Flat-plate Under Thermal Environments. *Int. J. Appl. Mech.* **2012**, *4*, 1250028. [CrossRef]
20. Geng, Q.; Li, H.; Li, Y. Dynamic and Acoustic Response of a Clamped Rectangular Plate in Thermal Environments: Experiment and Numerical Simulation. *J. Acoust. Soc. Am.* **2014**, *135*, 2674–2682.
21. Liu, Y.; Li, Y. Vibration and Acoustic Response of Rectangular Sandwich Plate Under Thermal Environment. *Shock Vib.* **2013**, *20*, 1011–1030. [CrossRef]
22. Rahmatnezhad, K.; Zarastvand, M.R.; Talebitooti, R. Mechanism study and power transmission feature of acoustically stimulated and thermally loaded composite shell structures with double curvature. *Compos Struct.* **2021**, *276*, 114557.
23. Zhang, G.; Ge, J. Vibration and Acoustic Radiation Characteristics of Simply Supported Curved Plate in Thermal Environment. *Arch. Appl. Mech.* **2022**, *92*, 3163–3177.
24. Li, X.; Yu, K.; Zhao, R.; Han, J.; Song, H. Sound Transmission Loss of Composite and Sandwich Panels in Thermal Environment. *Compos. Part B Eng.* **2018**, *133*, 1–14. [CrossRef]
25. Xin, F.X.; Gong, J.Q.; Ren, S.W.; Huang, L.X.; Lu, T.J. Thermoacoustic Response of a Simply Supported Isotropic Rectangular Plate in Graded Thermal Environments. *Appl. Math. Modell.* **2017**, *44*, 456–469.
26. Haddadpour, H.; Mahmoudkhani, S.; Navazi, H.M. Free Vibration Analysis of Functionally Graded Cylindrical Shells Including Thermal Effects. *Thin Walled Struct.* **2007**, *45*, 591–599.
27. Guo, L.; Ge, J.; Liu, S. Analysis of Vibration and Acoustic Characteristics of a Simply Supported Double-Panel Partition Under Thermal Environment. *Shock Vib.* **2020**, *2020*, 5613232. [CrossRef]
28. Gatewood, B.E. *Thermal Stresses*; McGraw-Hill: New York, NY, USA, 1957.
29. Flügge, W. *Statik and Dynamik der Schalen*; Springer: Berlin, Germany, 1957.
30. Soedel, W. *Vibrations of Shells and Plates*; Marcel Dekker: New York, NY, USA, 1981.

31. Xin, F.X.; Lu, T.J.; Chen, C.Q. Sound Transmission Through Simply Supported Finite Double-Panel Partitions with Enclosed Air Cavity. *J. Vib. Acoust.* **2010**, *132*, 325–326.

32. Pellicier, A.; Trompette, N. A Review of Analytical Methods, based on the Wave Approach, to Compute Partitions Transmission Loss. *Appl. Acoust.* **2007**, *68*, 1192–1212. [CrossRef]

33. Lin, G.; Guo, H.G.; Zhao, Y.T. *Aluminum Alloy Application Manual*; Mechanical Industry Press: Beijing, China, 2006.

34. Papadopoulos, C.I. Development of an Optimised, Standard-Compliant Procedure to Calculate Sound Transmission Loss: Numerical Measurements. *Appl. Acoust.* **2003**, *64*, 1069–1085.

35. Lee, J.-H.; Kim, J. Analysis of Sound Transmission Through Periodically Stiffened Panels by Space-Harmonic Expansion Method. *J. Sound Vib.* **2002**, *251*, 349–366. [CrossRef]

36. Wallace, C.E. Radiation Resistance of a Rectangular Panel. *J. Acoust. Soc. Am.* **1972**, *51*, 946–952. [CrossRef]

37. Cortés, F.; Elejabarrieta, M.J. Structural Vibration of Flexural Beams with Thick Unconstrained Layer Damping. *Int. J. Solids Struct.* **2008**, *45*, 5805–5813. [CrossRef]

38. Jeyaraj, P.; Ganesan, N.; Padmanabhan, C. Vibration and Acoustic Response of a Composite Plate with Inherent Material Damping in a Thermal Environment. *J. Sound Vib.* **2009**, *320*, 322–338. [CrossRef]